Earth and Planetary Science Letters 479 (2017) 50–59

Contents lists available at ScienceDirect

Earth and Planetary Science Letters

www.elsevier.com/locate/epsl

Response of the Amazon rainforest to late Pleistocene climate variability

Christoph Häggi [a,*], Cristiano M. Chiessi [b], Ute Merkel [a], Stefan Mulitza [a], Matthias Prange [a], Michael Schulz [a], Enno Schefuß [a]

[a] MARUM – Center for Marine Environmental Sciences, University of Bremen, Leobener Str. 8, 28359 Bremen, Germany
[b] School of Arts, Sciences and Humanities, University of São Paulo, Av. Arlindo Bettio 1000, 03828-000 São Paulo SP, Brazil

ARTICLE INFO

Article history:
Received 28 April 2017
Received in revised form 29 July 2017
Accepted 2 September 2017
Available online 2 October 2017
Editor: H. Stoll

Keywords:
Amazon
rainforest
paleoclimate
late Pleistocene
biodiversity
long-chain *n*-alkanes

ABSTRACT

Variations in Amazonian hydrology and forest cover have major consequences for the global carbon and hydrological cycles as well as for biodiversity. Yet, the climate and vegetation history of the lowland Amazon basin and its effect on biogeography remain debated due to the scarcity of suitable high-resolution paleoclimate records. Here, we use the isotopic composition (δD and δ^{13}C) of plant-waxes from a high-resolution marine sediment core collected offshore the Amazon River to reconstruct the climate and vegetation history of the integrated lowland Amazon basin for the period from 50,000 to 12,800 yr before present. Our results show that δD values from the Last Glacial Maximum were more enriched than those from Marine Isotope Stage (MIS) 3 and the present-day. We interpret this trend to reflect long-term changes in precipitation and atmospheric circulation, with overall drier conditions during the Last Glacial Maximum. Our results thus suggest a dominant glacial forcing of the climate in lowland Amazonia. In addition to previously suggested thermodynamic mechanisms of precipitation change, which are directly related to temperature, we conclude that changes in atmospheric circulation are crucial to explain the temporal evolution of Amazonian rainfall variations, as demonstrated in climate model experiments. Our vegetation reconstruction based on δ^{13}C values shows that the Amazon rainforest was affected by intrusions of savannah or more open vegetation types in its northern sector during Heinrich Stadials, while it was resilient to glacial drying. This suggests that biogeographic patterns in tropical South America were affected by Heinrich Stadials in addition to glacial–interglacial climate variability.

1. Introduction

Lowland Amazonia is covered by the largest and most biodiverse rainforest on Earth and is one of the major centers of tropical deep convection (Fig. 1) (Olson et al., 2001; Werth and Avissar, 2002). Hence, environmental changes in lowland Amazonia have major implications for the global carbon and hydrologic cycles (Brienen et al., 2015; Werth and Avissar, 2002). To predict the potential response of Amazonian vegetation and precipitation to future global climate shifts, a firm comprehension of past variability is critical. Especially the responses of Amazonian environmental conditions to Pleistocene glaciations, characterized by large changes in atmospheric greenhouse gas concentrations, and to abrupt shifts in the North Atlantic and global climate, are of great interest (Cheng et al., 2013; Kanner et al., 2012; Wang et al., 2017). While glacial–interglacial variability can be used to study the impact of large global temperature and sea level variations, millennial-scale variability such as Heinrich Stadials (HS) can be used to determine the impacts of variations in ocean circulation and shifts in the meridional position of the tropical rain belt.

Due to the scarcity of high-resolution climate records, there are conflicting scenarios regarding the late Pleistocene vegetation and climate history of lowland Amazonia (Cheng et al., 2013; Colinvaux et al., 1996; D'Apolito et al., 2013; Haffer, 1969; Kanner et al., 2012; Mosblech et al., 2012; Wang et al., 2017). Early studies based on biogeographic observations proposed that savannah expansion during glacial periods led to the formation of isolated forest refugia, where speciation took place ("refugia hypothesis") (Haffer, 1969). This scenario was initially supported by lacustrine pollen records from the fringes of the Amazon basin (Absy, 1991). However, first records from the interior of the Amazon basin (Hill of Six Lakes, Fig. 1) and marine sediment cores from the Amazon fan indicated that the Amazon rainforest persisted through colder and potentially drier conditions during

* Corresponding author.
E-mail address: chaeggi@marum.de (C. Häggi).

http://dx.doi.org/10.1016/j.epsl.2017.09.013
0012-821X/

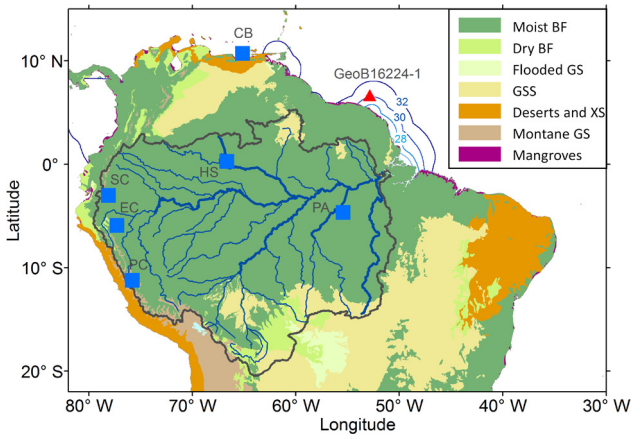

Fig. 1. Map of the Amazon basin and the adjacent Atlantic Ocean. Color shading represents the major modern-day biomes in tropical South America (Olson et al., 2001) (BF: Broad leaf forest; GS: Grassland and savannah; GSS: Grassland savannah and shrub land; XS: Xeric shrub land). The Amazon basin is outlined by a black line. Blue contour lines in the Atlantic Ocean represent sea surface salinity indicating the northward flow of Amazonian freshwater (Sbrocco and Barber, 2013). The location of core GeoB16224-1 is marked with a red triangle. The location of the other paleoclimate records from the Cariaco basin (CB) (Deplazes et al., 2013), the Santiago (SC) (Mosblech et al., 2012), El Condor (EC) (Cheng et al., 2013), Pacupahuain (PC) (Kanner et al., 2012) and Paraíso (PA) (Wang et al., 2017) caves, and the Hill of Six Lakes (HS) (Colinvaux et al., 1996) discussed in this study are marked with blue squares. (For interpretation of the references to color in this figure legend, the reader is referred to the web version of this article.)

the late Pleistocene (Boot et al., 2006; Colinvaux et al., 1996; Haberle and Maslin, 1999). These records are, however, controversial due to their low temporal resolution, the presence of hiatuses and the potential overprint by gallery forests (Behling et al., 2009; D'Apolito et al., 2013). Meanwhile, phylogenetic studies have found no evidence for increased speciation during the Pleistocene that would have supported the refugia hypothesis (Hoorn et al., 2010; Smith et al., 2014). In western Amazonia, where biodiversity is highest, various climate records showed humid conditions through Pleistocene glaciations, indicating that species richness was rather the consequence of long-term stability than of repeated vegetation shifts (Baker and Fritz, 2015; Cheng et al., 2013; Mosblech et al., 2012; Smith et al., 2014). Nevertheless, the close relation of species inhabiting savannah regions to the north and south of the lowland basin suggests the presence of temporary dry corridors through lowland Amazonia (Behling et al., 2009; Quijada-Mascareñas et al., 2007). Recently, a speleothem record from Paraíso Cave in the eastern part of the lowland basin again indicated drier glacial conditions leading to the conclusion that changes in temperature, associated with variations in atmospheric CO_2 were the dominant forcing mechanism controlling lowland Amazonian hydrology (Wang et al., 2017). The millennial-scale hydrologic variability in this record has also led to speculation on the potential impact of abrupt climate shifts on the former connection of biomes north and south of the basin (Bush, 2017). However, high-resolution vegetation records to confirm this link are lacking. Moreover, it is unclear what forcing mechanisms are dominant on a lowland basin-wide scale. This highlights the need for proxy records reflecting the integrated lowland Amazonian vegetation and climate evolution.

Here we provide high-resolution plant-wax isotope records from a marine sediment core collected offshore the Amazon River (Fig. 1) to reconstruct the catchment-integrated vegetation and climate conditions in the lowland Amazon basin for the late Pleistocene (50,000–12,800 yr before present). Plant-wax biomarkers in the Amazon River predominantly originate from the lowland basin and broadly reflect catchment-integrated signals (Häggi et al., 2016; Ponton et al., 2014). The stable hydrogen isotope composition of plant-waxes has been employed to reconstruct the isotopic composition of precipitation and thereby past precipitation amounts in tropical areas (e.g. Schefuß et al., 2005; Tierney and deMenocal, 2013; Tierney et al., 2008). The stable carbon isotope composition of plant-waxes allows to differentiate between biomes with dominant C3 or C4 vegetation and thus to study potential savannah expansions in the past (Castañeda and Schouten, 2011). Therefore, the isotopic plant-wax based approach allows us to perform climate and vegetation reconstructions that integrate changes from spatially extensive areas in the lowland basin and circumvents the spatial limitations of previous records. Moreover, our approach allows to independently assess changes in vegetation and precipitation on the same compounds. Finally, we compare our paleoclimate reconstructions to results from a fully coupled general circulation model, which provide insight into processes controlling regional hydroclimatic changes.

2. Materials and methods

2.1. Present-day climate conditions in the Amazon basin

In the lowland Amazon basin, mean annual precipitation varies between 1500 and 3000 mm/yr and mean annual temperatures reach values between 24 and 28 °C, while drier and cooler conditions are found in the Andean sector of the basin (Hijmans et al., 2005). With exception of some north-western parts of the Amazon basin, which experience year-round precipitation, most of the Amazon basin is subject to substantial seasonal precipitation variations. The highest precipitation amounts in the southern and central Amazon basin are registered during the maximum of the South American Monsoon, which peaks during austral summer in January and leads to humid conditions over most of the basin (Garreaud et al., 2009). During peak monsoonal conditions, large amounts of humid air are transported by the South American Low-Level Jet along the eastern slopes of the Andes to the south (Marengo et al., 2004). Convection over the Amazon basin also connects to the South Atlantic Convergence Zone over south-eastern Brazil, leading to intense local precipitation (Carvalho et al., 2004). During boreal spring, convection moves northwards following the seasonal insolation maximum until it reaches its northernmost position during boreal summer. In July, precipitation takes mostly place in the northern sector of the basin, where it is aligned with the position of the Intertropical Convection Zone. During October, convection again shifts southward and precipitation over the central Amazon basin and in the South Atlantic Convergence Zone re-intensifies (Garreaud et al., 2009).

2.2. Study area and sample material

Paleoenvironmental reconstructions for the Amazon basin presented in this study are based on sediment core GeoB16224-1 (6°39.38′N, 52°04.99′W; 760 cm core length; 2510 m water depth) retrieved from the continental margin off French Guiana during *RV MS Merian* cruise MSM20/3 in February 2012 (Mulitza et al., 2013). While in the present-day sedimentological setting most of the Amazonian freshwater and sediment is transported along the continental shelf (Geyer et al., 1996), sedimentation during glacial sea-level low stands took place on the continental margin (Damuth and Flood, 1983). During glacial times, well-stratified sediment deposits formed on the continental margin off French Guyana and represent high-resolution archives for paleoclimate reconstructions (Loncke et al., 2009; Mulitza et al., 2013). A previous study on GeoB16224-1 showed that the core site received continuous fine-grained sedimentary input from the Amazon Plume from 50 kiloyears (ka) before present (BP) until the end of the Bølling–Allerød (12.8 ka BP) when rising sea levels shifted the main depositional

area onto the shelf (Zhang et al., 2015). Using Nd isotopes Zhang et al. (2015) also showed that alternative sources such as smaller local rivers or Saharan dust import are unlikely to have influenced sedimentation at the core site. Since there is no present-day sedimentation at the core site that could be used to describe modern conditions, we compared the down-core results to published core-top data from GeoB16212-3 (3°06.27′N, 49°23.28′W; 75 m water depth) from the Amazon shelf, where present-day deposition of Amazonian sediments is taking place (Häggi et al., 2016; Mulitza et al., 2013).

For this study, sediment samples for compound-specific $\delta^{13}C$ and δD analyses of *n*-alkanes were collected in 4-cm intervals (i.e. 1 cm sample with 3 cm left in between) from GeoB16224-1, yielding an average temporal resolution of approximately 250 yr. A total of 180 samples with a dry weight between 8 and 18 g were collected for proxy analysis.

2.3. Age model

To produce the age model for core GeoB16224-1, we used 15 ^{14}C AMS ages of planktonic foraminifera from Zhang et al. (2015). Since there is a large gap in ages between 50 and 66 cm, suggesting the presence of a hiatus, we did not use the upper 66 cm of the core. In the radiocarbon-dated section of the core, the XRF record from Zhang et al. (2015) shows distinct peaks during Heinrich Stadials. Since HS are also recorded in absolutely U/Th dated speleothem records from the Amazonian Andes this allows to extend the age model of GeoB16224-1 beyond the radiocarbon limit by correlating HS of the XRF record to the Andean speleothem chronology (Supplementary Fig. S1). Hence, in the lowermost part of the core, where radiocarbon dating reached the limits of its applicability, the age model was amended by tying the HS5 peak in the XRF data (Zhang et al., 2015) to the absolutely U/Th dated speleothem chronology of speleothem ELC-B from El Condor Cave in the Amazonian Andes (Cheng et al., 2013). The age model was established using Bayesian modeling conducted with the R-script BACON (Blaauw and Christen, 2011). Calibrated ^{14}C ages were adapted from Zhang et al. (2015), where calibration was achieved with the Marine13 calibration curve (Reimer et al., 2013). The error for the tie point to the speleothem U/Th chronology was used without modification from Cheng et al. (2013). The BACON script was applied with default parameters, except for *acc.mean*, which was changed to 50 $y\,cm^{-1}$, to more closely reflect the average accumulation than the default setting of 20 $y\,cm^{-1}$. 10,000 age–depth relations generated with Bacon were used to calculate the median age and the uncertainty envelope (Supplementary Fig. S2). Values generated during the burn-in were excluded from consideration.

2.4. Methodological approach

The isotope measurements presented in this study are based on long-chain *n*-alkanes. These compounds are mostly produced by leaves of vascular plants (Eglinton and Hamilton, 1967). In the Amazon basin, there is also a minor petrogenic source for long-chain *n*-alkanes on top of modern vegetation (Häggi et al., 2016). To monitor potentially large variations in the influx of petrogenic and degraded *n*-alkanes, the relative abundance of these compounds was analyzed. There are various factors that can influence the relative abundance of compounds. Among others, large scale variations in the input of petrogenic or degraded material to the core site would likely manifest in major shifts in the relative abundance of long-chain *n*-alkanes. To detect potential variations, two different indices were applied. On the one hand, the average chain length of the compounds with a chain-length between 27 and 33 carbon atoms (ACL_{27-33}, for formulas see Häggi et al., 2016) is influenced by petrogenic input or compounds from higher altitude (Häggi et al., 2016; Feakins et al., 2016). On the other hand, the carbon preference index (CPI_{26-34}) describing the ratio between compounds of odd and even chain length can be used to trace degraded material (Cranwell, 1981). Even though these indices cannot be used quantitatively, they would likely show a response if large changes in the relative amount of petrogenic or degraded material would occur throughout the record.

Previous studies showed that the source region of organic matter (Bouchez et al., 2014) and plant-waxes is distributed throughout the lowland Amazon basin (Häggi et al., 2016; Ponton et al., 2014). This contrasts the dominant Andean sourcing of inorganic sediments (Meade et al., 1985). Even though the source region of plant-waxes can be constrained to the lowland basin, there is still the possibility of a bias towards certain parts of the lowland basin, especially the extensive floodplains. Since the present-day signal at the Amazon estuary integrates compounds with varying isotope composition from different regions (Häggi et al., 2016), changes in the source region could also have a considerable impact on isotope variations in the record. Seasonal variations in plant-wax composition have been shown to impact the plant-wax isotope composition in the Andean headwaters (Ponton et al., 2014), but seem to be leveled out during transport (Häggi et al., 2016).

Studies using riverine sediment for the reconstruction of dominant vegetation in river catchments are often regarded to be disproportionally influenced by gallery forest that could mask savannah contributions from the hinterland. Even though gallery forests could lead to a bias in $\delta^{13}C$ values towards forest vegetation, they are unlikely to fully mask potential savannah contributions. In the neighboring Parnaíba River basin, for instance, present-day vegetation features a mix of C3 and C4 species (Caatinga and Cerrado vegetation types) (Pennington et al., 2000), with gallery forests along the rivers. Data from marine core-tops offshore the Parnaíba basin show a clear ^{13}C enrichment (Häggi et al., 2016) and thus indicate that a mixed C3/C4 vegetation in the hinterland leads to a ^{13}C enrichment in transported signals even in the presence of gallery forests.

2.5. Lipid analysis

Lipid extraction and separation procedures followed the same protocol as described in Häggi et al. (2016). Quantification of long-chain *n*-alkanes was achieved using a ThermoFisher Scientific Focus gas chromatograph equipped with an Rxi-5 ms 30x column (30 m, 0.25 mm, 0.25 µm) and a flame ionization detector. Compound-specific δD analyses were conducted in duplicates on a ThermoFisher Scientific MAT 253 isotope ratio mass spectrometer (IRMS) coupled via a GC Isolink operated at 1420 °C to a ThermoFisher Scientific Trace GC equipped with an HP-5ms column (30 m, 0.25 mm, 1 µm). δD compositions were measured against calibrated H_2 reference gas and precision was controlled by external *n*-alkane standards of known isotopic composition (chain length: nC_{16}–nC_{34}; isotope composition −261 to −31‰). The H_3^+ factor was determined daily and varied between 5.3 and 5.9 over the measurement period. Accuracy in each measurement was controlled by an internal squalene standard (isotopic composition -180.3 ± 2.3‰). The deviation from the target value of the internal squalene standard was -1.1 ± 1.5‰. Compound-specific stable carbon isotope analyses were carried out in duplicates on a ThermoFisher Scientific MAT 252 isotope ratio mass spectrometer coupled via a GCC combustion interface with a nickel catalyzer operated at 1000 °C to a ThermoFisher Scientific Trace GC equipped with an HP-5ms column (30 m, 0.25 mm, 0.25 µm). $\delta^{13}C$ values were calibrated against CO_2 reference gas of known isotopic composition and precision was controlled by measuring *n*-alkane

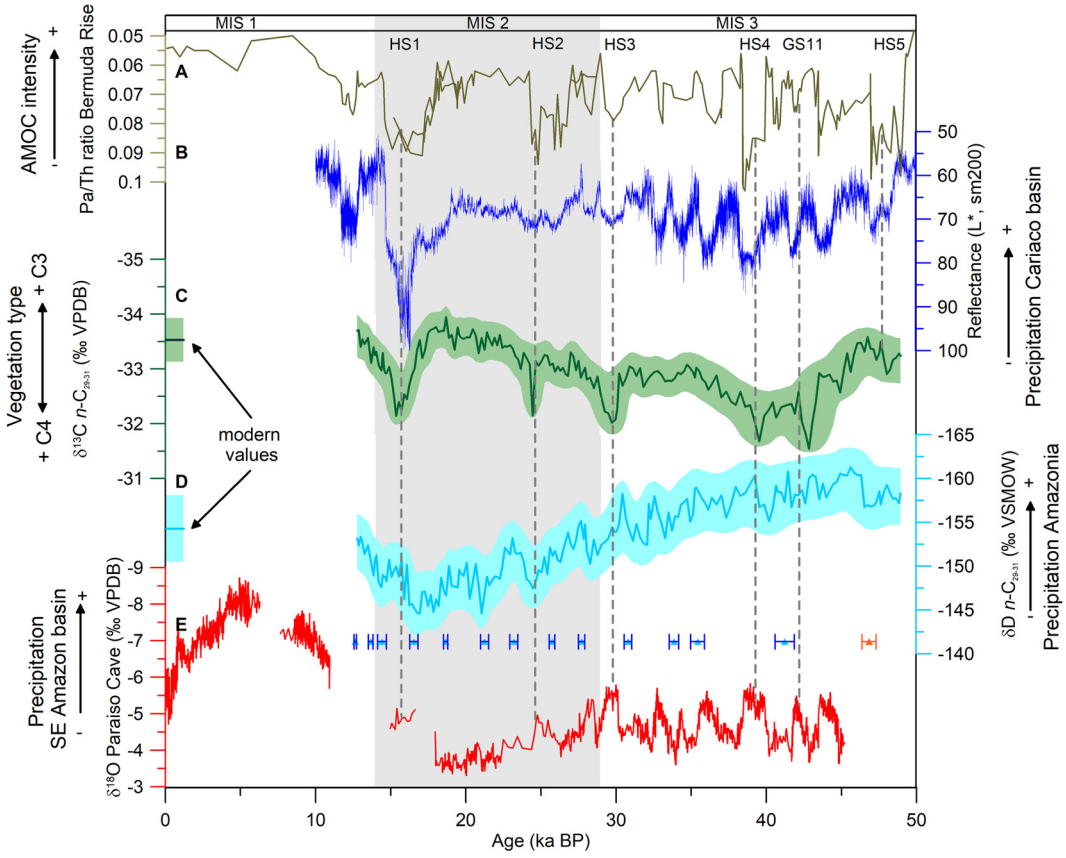

Fig. 2. Precipitation and vegetation reconstructions for lowland Amazonia and other hydroclimate records from tropical South America. (A) Intensity of the Atlantic meridional overturning circulation (AMOC) as indicated by the Pa/Th ratio from the Bermuda rise (Henry et al., 2016; Lippold et al., 2012; McManus et al., 2004). (B) Color reflectance from the Cariaco basin indicating the relative amount of terrestrial sediment input and the position of the tropical convection center in northern South America (Deplazes et al., 2013). (C) δ^{13}C n-C_{29-31} of core GeoB16224-1 (this study). The core top value for GeoB16212-3 from the Amazon outflow is plotted on the left of the figure (Häggi et al., 2016). (D) δD n-C_{29-31} of core GeoB16224-1 (this study). The core top value for GeoB16212-3 from the Amazon outflow is given on the left of the figure (Häggi et al., 2016). (E) δ^{18}O data from Paraíso Cave (corrected for the ice volume effect) indicating the precipitation amount in the south-eastern Amazon basin (Wang et al., 2017). The gray bar indicates the duration of marine isotope stage 2 (MIS2). The timing of Heinrich Stadials (HS) 1–5 and Greenland Stadial (GS) 11 is indicated with vertical dashed lines. Blue triangles indicate the calibrated ^{14}C AMS ages with 2σ error bars from core GeoB16224-1 (Zhang et al., 2015). The orange triangle represents the tie point to the U/Th dated El Condor speleothem record (Cheng et al., 2013). Shaded areas in the isotope records indicate the combined 2σ uncertainty envelope of age and isotope values. (For interpretation of the references to color in this figure legend, the reader is referred to the web version of this article.)

standards of known isotopic composition (chain length: nC$_{16}$–nC$_{34}$; isotope composition −33 to −19‰) every six measurements. Accuracy in each measurement was also controlled by the internal squalene standard (isotopic composition: -19.72 ± 0.18‰). Here, the deviation of the internal squalene standard from the target value was -0.34 ± 0.15‰.

2.6. Error estimation and ice volume correction

Error estimates for the isotope measurements are based on the analysis of multiple standards interspersed between measurements. To deduce the error of the isotope measurements, the difference between standard and theoretical value (long-term mean of the standard) was analyzed. For the stable hydrogen isotope measurements, the standard mixture included compounds of chain-length between 16 and 34 carbon atoms and squalane (a total of 16 different compounds) and covered an isotopic range between −261 to −31‰. For the error estimation, the results of 228 standard runs each including 16 different components and thus a total of 3648 isotope values were used. The difference between the measured isotope value ($\delta D_{std\ measured}$) and the target value (δD_{std}) defined as

$$\Delta\delta D_{std} = \delta D_{std\ measured} - \delta D_{std} \quad (1)$$

indicates that $\Delta\delta D_{std}$ follows a normal distribution with a standard deviation of 1.9‰. The error for δ^{13}C measurements was analyzed analogously using the same standard solution covering isotope values between −33 and −19‰. In the case of δ^{13}C measurements a total of 3456 isotope values yielded a standard deviation of 0.20‰.

To integrate the isotope measurement errors with the error of the age model, 10,000 Monte Carlo proxy-time series realizations based on the BACON-age model error and the isotope errors (i.e., a 1σ-error estimate of 1.9‰ for δD and 0.20‰ for δ^{13}C) were modeled. The reported error envelopes shown in the results are thus representative of both the age and isotope measurement uncertainty.

Due to the accumulation of the lighter hydrogen isotope (^{1}H) in continental ice sheets during the last glacial, the mean isotopic composition of hydrogen in the rest of the global hydrological cycle became more ^{2}H-enriched (by 8‰ on average) compared to present-day conditions (Bintanja et al., 2005). This ice-volume effect was accounted for by applying the following ice volume correction (IVC) (Tierney and deMenocal, 2013):

$$\delta D_{wax\text{-}IVC} = \frac{1000 + \delta D_{wax}}{8 * 0.001 * \delta^{18}O_{isoice} + 1} - 1000 \quad (2)$$

where $\delta D_{wax\text{-}IVC}$ represents the ice volume corrected isotope values, δD_{wax} the measured δD of plant-waxes and $\delta^{18}O_{isoice}$ the effect of ice volume on the benthic δ^{18}O variation (Bintanja et al., 2005). For reasons of comparability to our data, an analogous cor-

rection was applied to the speleothem $\delta^{18}O$ record shown in Fig. 2 (Wang et al., 2017).

2.7. Climate model simulations

A detailed description of the numerical climate model setup and experimental design is given in Merkel et al. (2010). Here we provide a short description of the conducted experiments. We used the fully-coupled general circulation model CCSM3 (Community Climate System Model version 3; Collins et al., 2006). In our experiments, the atmospheric component has a 3.75° (T31) horizontal resolution with 26 layers in the vertical and is coupled to an ocean model with nominal 3° horizontal resolution and 25 levels (Yeager et al., 2006). For the different experiments, boundary conditions for the pre-industrial, the Last Glacial Maximum (LGM), and the 35 ka time slice (MIS3) were applied. These boundary conditions take atmospheric greenhouse gas concentrations, ice-sheet configurations, astronomical parameters, and land–sea distribution due to sea level changes into account. Pre-industrial and LGM boundary conditions follow the guidelines of the Paleoclimate Modeling Intercomparison Project phase 2 (Braconnot et al., 2007). The performed HS1 experiment uses the LGM setup with an additional constant freshwater hosing of 0.2 Sv (1 Sv $= 10^6$ m^3/s) into the northern North Atlantic to disturb the Atlantic Meridional Overturning Circulation (AMOC). A smaller and negative freshwater forcing (−0.1 Sv) was applied to the MIS3 simulation in order to obtain two different MIS3 climate states, a weak-AMOC stadial (MIS3 ST) and a strong-AMOC interstadial (MIS3 IST) state. All simulations were run into quasi-equilibria and long-term means were used for the analysis of climate variables. The AMOC strengths (as measured by the Atlantic overturning stream function at 25°S) in these experiments are 11.6 (pre-industrial), 2.7 (HS1), 10.1 (LGM), 6.6 (MIS3 ST), and 14.1 Sv (MIS3 IST).

For this study we analyzed the different factors controlling precipitation change in the Amazon basin. To that end, mean precipitation, total precipitable water (i.e., column-integrated water vapor) and the intensity of tropospheric vertical velocity at the 500 hPa level (ω500) were averaged over the Amazon region (72°W to 48°W; 12°S to 3°N). Tropospheric vertical velocity correlates with convective mass flux and was used to infer the influence of changes in convection on precipitation in the Amazon basin (Vecchi and Soden, 2007).

3. Results

The analysis of long-chain *n*-alkanes in GeoB16224-1 showed that the concentrations of the dominant long-chain C_{29} and C_{31} *n*-alkanes varied between 0.1 and 0.7 µg/g dry sediment. The relative abundance of different *n*-alkane compounds as indicated by ACL_{27-33} and CPI_{26-34} ratios remained stable throughout the entire record. ACL_{27-33} values varied between 29.8 and 30.4, while CPI_{26-34} values were between 3.4 and 5.7 (Supplementary Fig. S3).

Our vegetation reconstruction based on the $\delta^{13}C$ of *n*-C_{29} and *n*-C_{31} alkanes ($\delta^{13}C$ *n*-C_{29-31}) shows values between −31.5‰ and −34‰ vs. VPDB (Fig. 2c, Supplementary Fig. S4b). The most depleted values of −34‰ are found during the Last Glacial Maximum (LGM) and in the period before 45 ka BP. There is a small long-term trend to more enriched values of around −32.5‰ from 45 to 42 ka BP and a trend back towards more depleted values from 38 to 20 ka BP. Compared to the modern values found in the core-top of GeoB16212-3 (Häggi et al., 2016), most of the $\delta^{13}C$ *n*-C_{29-31} record is similar or only slightly more enriched suggesting that lowland Amazonia remained largely forest covered from 50 to 12.8 ka BP (Fig. 2c). The most enriched $\delta^{13}C$ *n*-C_{29-31} values in our record are found in distinct peaks of up to −31.5‰ coinciding with HS 1–4 and likely coinciding with Greenland Stadial 11 (Fig. 2c).

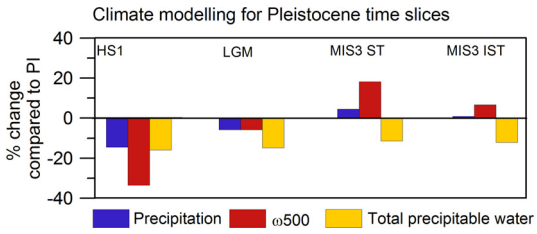

Fig. 3. Relative changes in modeled precipitation, convection and total precipitable water over the Amazon basin (72°W to 48°W; 12°S to 3°N). Bar-charts for each time slice (i.e., Heinrich Stadial 1 (HS1), the Last Glacial Maximum (LGM) and marine isotope stage 3 stadial (MIS3 ST) and interstadial (MIS3 IST) conditions at 35 ka BP) represent relative changes (in %) with respect to pre-industrial (PI) conditions for simulated precipitation, atmospheric vertical velocity at the 500 hPa level (ω500) and total precipitable water averaged over the Amazon basin. Total precipitable water is used as an indicator of atmospheric moisture content, while ω500 is used as a measure for convection intensity. Model results are long-term annual means based on the last 100 yr of each simulation (Merkel et al., 2010).

The average δD for the dominant *n*-C_{29} and *n*-C_{31} *n*-alkanes corrected for ice-volume changes (δD *n*-C_{29-31}) found in core GeoB16224-1 during marine isotope stage (MIS) 3 shows values similar to the core-top from GeoB16212-3 (−155‰ vs. VSMOW) (Fig. 2d, Supplementary Fig. S4) (Häggi et al., 2016). Towards the LGM there is a gradual enrichment of 15‰. During the deglaciation, δD *n*-C_{29-31} became again more depleted. On millennial timescales, the δD record shows only limited variability.

The CCSM3 experiments show that precipitation amounts over the Amazon Basin were lower during the HS1 and LGM time slices compared to the pre-industrial, while the MIS3 stadial and interstadial time-slices show conditions comparable to the pre-industrial. Precipitable water over the Amazon was consistently lower during all the late Pleistocene time-slices compared to pre-industrial (Fig. 3). Vertical atmospheric velocity at the 500 hPa level, used as a measure for convection, was weaker compared to the pre-industrial during the HS1 and LGM time-slices and stronger during MIS3 stadial and interstadial conditions.

4. Discussion

4.1. Reconstruction of Amazonian vegetation

Since the CPI_{26-34} and ACL_{27-33} values found in GeoB16224-1 show only little variability, the degree of degradation of *n*-alkanes seems to be rather constant throughout the record. The input of petrogenic material cannot be ruled out completely, but seems at least to be stable over the entire record and thus not responsible for the variability in our isotope records. As we do not find any indication for variations in petrogenic input, we interpret shifts in *n*-alkane isotope composition as a vegetation-derived signal from the Amazon basin.

Our vegetation reconstruction based on the $\delta^{13}C$ *n*-C_{29-31} shows only minor variability for most of the record with values that are in the range of modern core-top sediment from the Amazon shelf (GeoB16212-3; Häggi et al., 2016). Thus, our $\delta^{13}C$ record indicates that most of the Amazon basin remained forest covered during the late Pleistocene. Maximal enrichment in $\delta^{13}C$ *n*-C_{29-31} occurred during HS and showed values of up to −31.5‰ (Fig. 2c). A shift to full C4 vegetation would have led to values around −22‰ (Castañeda and Schouten, 2011). However, South American Cerrado and Caatinga vegetation types do not exclusively feature C4 vegetation and represent a mix of C3 and C4 plants (Pennington et al., 2000). Therefore, a shift to full C4 vegetation is not to be expected, even if the Amazon rainforest would have been fully replaced with South American savannah types. A shift to a mixed vegetation

with savannah and gallery forests as found today in north-eastern Brazil would have led to more enriched values between −27‰ and −29‰ (Häggi et al., 2016). Since the most enriched values during HS are intermediate between the present-day Amazon rainforest and northeastern Brazil, they indicate only a partial replacement of the Amazon rainforest by mixed vegetation types or savannah during HS.

Apart from a shift towards more C4 vegetation, the ^{13}C enrichment found during HS could also be the consequence of variations in the canopy effect and shifts to C3 species with better water use efficiency and lower stomatal conductance (Diefendorf et al., 2010). The canopy effect describes the observation that $\delta^{13}C$ values in dense forest systems can show very depleted values due to the uptake of recycled CO_2 from degraded biomass on the forest floor (van der Merwe and Medina, 1991). Since a decrease in the canopy effect due to a more open forest vegetation and shifts in the C3 species composition towards better adaptation to drier conditions would both lead to more enriched values, they would act in the same direction as shifts from C3 to C4 vegetation types.

The maxima in more open vegetation types potentially featuring C4 vegetation occurrence were most likely caused by southward shifts of the tropical convection center evident in climate records from northern South America (Cariaco basin) (Deplazes et al., 2013) and parts of the Amazon basin south of the equator (Cheng et al., 2013; Kanner et al., 2012; Mosblech et al., 2012; Wang et al., 2017) (Fig. 2b, e). The southward shift of the tropical convection center in turn is related to a slowdown in the Atlantic Meridional Overturning Circulation (AMOC) (Fig. 2a) (McManus et al., 2004; Lippold et al., 2012; Henry et al., 2016). As a consequence of a southward shift of the convection center, savannah expansion most likely occurred in the northern sector of the Amazon basin.

Our finding of rapid vegetation shifts in the northern Amazon Basin is also in line with the vegetation response to millennial-scale climate variability observed in sediment cores from the Cariaco basin (Hughen et al., 2004). Due to a southward shift of the tropical rain belt, there was likely forest expansion in the savannah regions southeast of the basin. In part, this forest expansion took place outside the Amazon basin (i.e., in northeastern Brazil; Dupont et al., 2010) and did therefore not influence our Amazonian record. The conclusion that the $\delta^{13}C$ n-C_{29-31} enrichment during HS represents savannah expansion in the north of the Amazon basin is corroborated by the timing of events during HS1. During HS1, the ^{13}C enrichment peaks at 15.5 ka BP and coincides with the maximal southward displacement of the tropical rain belt over northern South America (Deplazes et al., 2013) (Supplementary Fig. S5c, d), while precipitation shifts in the Andean and lowland speleothem records influenced by the South American Summer Monsoon already started at 18 ka BP (Cheng et al., 2013; Wang et al., 2017; Mosblech et al., 2012) (Supplementary Fig. S5a). Likewise, the increase in the Fe/Ca ratio in GeoB16224-1 also takes place at 18 ka BP indicating enhanced Andean sediment input (Supplementary Fig. S5b, Zhang et al., 2015). The Fe/Ca ratio declines again at around 16 ka BP in step with Andean speleothem records when the Cariaco basin features the driest conditions (Supplementary Fig. S5a, b, c). The timing of events during HS1 thus indicates that the shifts in $\delta^{13}C$ n-C_{29-31} are not in direct connection with a precipitation increase in the Andes that may carry an enhanced amount of petrogenic compounds or compounds from higher altitude regions that also would show ^{13}C enrichment. Even though petrogenic material does not seem to be a dominant factor influencing our records, pre-aged material could potentially exert a minor influence.

Apart from the short-term vegetation variability there is also a small long-term trend between 45 and 20 ka BP visible in the $\delta^{13}C$ n-C_{29-31} record. This potentially reflects a development similar as in the Cariaco basin record that also shows some of the driest periods around HS4 (Fig. 2a). Alternatively, the long-term trend could be influenced by shifts in savannah vegetation in the southern sector of the Amazon basin (Absy, 1991; Mayle et al., 2000).

4.2. Reconstruction of Amazonian hydroclimate

While the amount effect presents one of the dominant factors controlling the isotope composition of precipitation in the Amazon basin, further effects have to be considered in the interpretation of δD variations, especially in the western parts of the Amazon basin (Brienen et al., 2012; Lee et al., 2009; Vuille et al., 2003; Wang et al., 2017). Changes in temperature, precipitation seasonality and moisture trajectory and source may also influence the isotope composition of precipitation (Lee et al., 2009; Vuille et al., 2003). Furthermore, variations in moisture recycling in the Amazon rainforest have also been noted to lead to variations in the isotope composition of precipitation in the western parts of the basin (Wang et al., 2017). While there were only limited variations in temperature in tropical South America from MIS2 to MIS3 (Jaeschke et al., 2007), changes in isotopic gradient, precipitation seasonality, moisture trajectory and moisture source are hard to constrain.

Despite the fact that δD of long-chain n-alkanes is mainly influenced by the δD of meteoric water, secondary effects might also contribute (Sachse et al., 2012). In arid regions, the δD of plant-waxes is reported to be additionally controlled by evapotranspirative enrichment of soil and leaf waters (Feakins and Sessions, 2010). Different vegetation types also show a wide range of fractionation factors (Sachse et al., 2012). Since our data shows that forest cover persisted throughout the late Pleistocene, evapotranspirative enrichment and changes in vegetation cover likely did not play a dominant role in defining the δD of plant-waxes in the Amazon rainforest. Even if small-scale evapotranspirative enrichment and shifts towards more open vegetation had occurred, this would have enhanced the isotopic enrichment caused by the lower precipitation amount and thus acted in the same direction as the amount effect. Since $\delta^{13}C$ values are relatively stable and variability in the $\delta^{13}C$ and δD records takes place on different time-scales, we do not expect variations in vegetation to be the dominant factor influencing our δD record.

Given that the δD of precipitation in the eastern sector is more D-enriched than in the western sector of the Amazon basin, more enriched values in our δD record could indicate an enhanced input of plant-waxes from the eastern sector of the basin. However, such an interpretation of our record is at odds with previous studies which indicate that precipitation in the Andes was high during the LGM (Cheng et al., 2013; Kanner et al., 2012; Mosblech et al., 2012). An enhanced input of material from the western part of the basin would have resulted in an increased input of more isotopically depleted compounds, which would contradict the more enriched isotope values in our δD record. Likewise, climate records from the eastern portion of the Amazon rainforest show dry conditions during the LGM (Absy, 1991; Wang et al., 2017), which makes an enhanced input of isotopically enriched compounds from the eastern basin unlikely. Apart from that, changes in vegetation could also lead to biases of material from certain regions. For instance, there could be less material from regions affected by savannah expansion, which would potentially lead to an underrepresentation of these regions in both the $\delta^{13}C$ and δD records.

Overall, changes in moisture trajectory, seasonality and isotopic gradient over the basin are the most likely factors to influence the δD n-C_{29-31} data besides the dominant amount effect. Secondary effects during plant-wax synthesis would likely act in the same di-

rection and thus amplify the amount effect signal, while changes in source area due to vegetation changes would potentially lead to an underestimation of the magnitude of vegetation variability. Since it is not possible to quantitatively disentangle the influence of the amount effect and possible changes in moisture trajectory, seasonality and variations in the isotope gradient on the δD data, we interpret the shifts in δD n-C_{29-31} to reflect qualitative changes in precipitation amount, moisture transport and isotopic gradient. The dominant long-term δD n-C_{29-31} trend from more depleted values during MIS3 to more enriched values during MIS2 thus suggests that there were distinct precipitation and circulation changes taking place from MIS3 to MIS2. The more enriched values during MIS2 are indicative of more arid conditions, but could also be influenced by changes in moisture trajectory and isotope gradient that took place on the same time-scale and were potentially interdependent with precipitation changes.

The timing of the trend in our δD n-C_{29-31} record indicates a dominant glacial forcing of lowland Amazonian hydrology. Millennial-scale variations appear to be muted, in contrast to the δ^{13}C n-C_{29-31} record (Fig. 2c). In the δD n-C_{29-31} record, drying in the north was likely offset by wetter conditions in the southern and western sectors of the basin (Kanner et al., 2012; Wang et al., 2017). Since proxy records to the north and the south of the South American tropical rain belt show little variation from MIS3 to MIS2, a meridional movement of the convection center is unlikely to be the cause for the long-term pattern (Deplazes et al., 2013).

Changes in both precipitation and circulation from MIS3 to MIS2 are supported by our model results. Based on the model output, we suggest that LGM rainfall reduction was caused by a combination of reduced atmospheric water vapor, decreasing the available moisture supply, and dynamical circulation change associated with reduced convective mass flux. The climate model results show a decrease of total precipitable water, i.e., column-integrated water vapor, for all late Pleistocene time-slices compared to the pre-industrial (Fig. 3). This is primarily controlled by a sea-surface temperature decrease and the reduced moisture-holding capacity of colder air (Chadwick et al., 2016). The intensity of vertical velocity at the 500 hPa level used as a measure for convective mass flux only decreased during HS1 and the LGM but increased during MIS3 leading to precipitation amounts comparable to the pre-industrial despite the drier air masses (Fig. 3). The weaker (stronger) vertical motion during MIS2 (MIS3) was likely related to the different ice-sheet heights during MIS3 and MIS2 which both induced a high-to-low latitude upper-tropospheric wave-like zonal wind anomaly pattern, but of opposite signs over the Amazon basin, thereby interfering with regional circulation in suppressing enhancing (MIS3) or suppressing (MIS2) convection. The finding that tropical convection decreased only during the glacial maximum conditions is in line with a suggested non-linear effect of changes in ice sheet topography on tropical precipitation (Lee et al., 2014). Furthermore, the conclusion of drier LGM conditions in our model is supported by previous regional model studies for the Amazon basin (e.g. Vizy and Cook, 2007).

4.3. Synthesis and comparison to existing paleoclimate records

Remarkably, the δ^{13}C n-C_{29-31} and δD n-C_{29-31} records show distinctly different modes of variability. While δ^{13}C n-C_{29-31} shows distinct short-term variability, the δD n-C_{29-31} record mainly features orbital time-scale variability with little short-term changes. Since both isotope measurements were conducted on the same compounds, this difference cannot be explained by different source regions but is rather a consequence of different factors reflected by each proxy. While the δ^{13}C n-C_{29-31} reconstructions represent regional precipitation or humidity thresholds below which more open vegetation types expand, the δD n-C_{29-31} reconstructions reflect continuous changes in basin-wide hydrology. Hence, the discrepancy of the two records can be explained by the rationale that regional expansion of more open vegetation types occurred in regions below a certain precipitation or humidity threshold, while in the rest of the basin the vegetation remained stable and did hence not influence $\delta^{13}C_{29-31}$, even if precipitation increased. Conversely, the δD n-C_{29-31} record is influenced by linear changes in precipitation δD values throughout the basin and decreased precipitation amounts in the north during HS were offset by increases in the south of the basin. As a consequence, the δ^{13}C record is much more susceptible to regional variations than the δD record in which regional variations are leveled out on a basin-wide scale.

Our combined vegetation and precipitation reconstructions thus indicate that the basin-averaged LGM drying was insufficient to cause large-scale replacement of forest by savannah vegetation. This confirms earlier suggestions about the resilience of Amazonian vegetation towards drier climate (Bush, 2017; Colinvaux et al., 1996; Haberle and Maslin, 1999; Wang et al., 2017). Our results further suggest that the most pronounced expansion of C4 vegetation took place during Heinrich Stadials due to local aridity in the northern sectors of the Amazon basin. This drying in the northern sector of the basin during HS contrasts the more humid conditions found in the southern sector (e.g. Wang et al., 2017; Mosblech et al., 2012). Since the more humid conditions in the south could not lead to a large-scale increase in the already present forest vegetation, they did not compensate for the enrichment in our δ^{13}C record. Major forest expansion was indeed taking place in tropical South America during HS, but was probably occurring largely in regions outside the Amazon basin such as north-eastern Brazil (Hessler et al., 2010; Dupont et al., 2010).

The inference of a dominant glacial forcing in controlling the lowland Amazonian climate broadly confirms the findings from the Paraíso δ^{18}O record, which is so far the only lowland isotope record from the Amazon Basin (Wang et al., 2017). There are, however, several differences between the Paraíso δ^{18}O record and our isotope records. If corrected for global ice volume changes, the baseline in the Paraíso record is relatively stable with a shift of 0.5‰ from MIS3 to MIS2, and shows millennial-scale variability during Greenland Stadials (Wang et al., 2017) (Fig. 2e). In contrast, we find that conditions during MIS3 in our δD record were more humid than during MIS2 (Fig. 2d). This suggests that there are additional factors which complement the temperature forcing of the lowland Amazonian hydrology deduced from the Paraíso record (Wang et al., 2017). Our results indicate that dynamic processes such as atmospheric circulation anomalies induced by ice sheet topography play an important role for the late Pleistocene climate evolution in lowland Amazonia.

Our suggestion that conditions during MIS3 were more humid than during MIS2 is supported by lake and geomorphological records from the lowland Amazon basin (D'Apolito et al., 2013; van der Hammen et al., 1992). The recent re-analysis of the lake records from the Hill of Six Lakes suggests that precipitation amounts were lowest during the LGM (D'Apolito et al., 2013), similar to lake records from the south-eastern and north-eastern parts of the basin (Absy, 1991; Colinvaux et al., 2001). The analysis and dating of river terraces from the northern and western parts of the basin also suggests that the driest conditions in lowland Amazonia were limited to the glacial maximum (Latrubesse and Franzinelli, 2005; van der Hammen et al., 1992).

Climate patterns with humid conditions during MIS3 and drying during the LGM have also been reported from the other major centers of tropical deep convection in Africa (Lake Tanganyika) and Indonesia (Lake Towuti) (Fig. 4) (Russell et al., 2014; Tierney et al., 2008). In both records, long-term variability displays a pattern similar to our δD n-C_{29-31} reconstruction, while

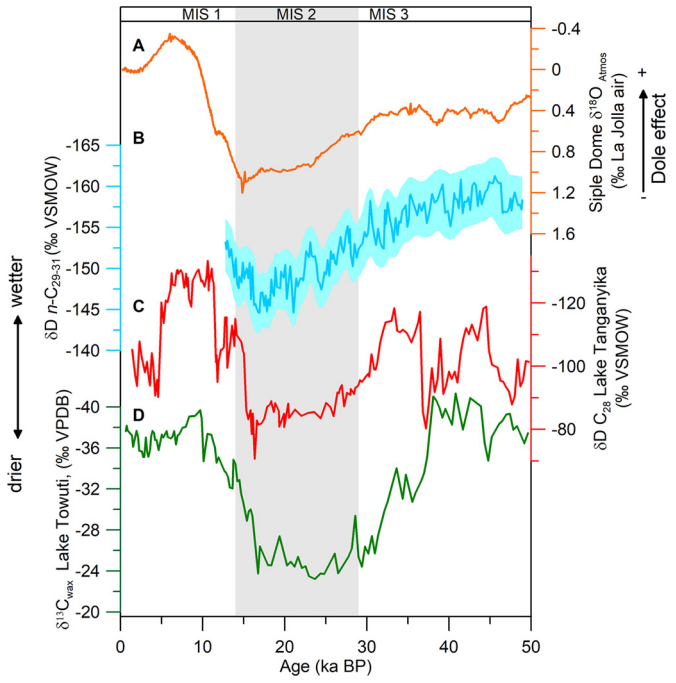

Fig. 4. Comparison to records from other tropical convection centers. (A) Atmospheric $\delta^{18}O$ from the Siple Dome (Severinghaus et al., 2009), reflecting the strength of the Dole effect (i.e., primary productivity in monsoonal regions and the tropics). (B) δD of nC_{29} and nC_{31} *n*-alkanes from lowland Amazonia (this study). (C) δD of the C_{28} *n*-carboxylic acid from Lake Tanganyika (Tierney et al., 2008). (D) $\delta^{13}C$ of the C_{26}, C_{28}, and C_{30} *n*-carboxylic acids from Lake Towuti, Sulawesi, indicating large-scale savannah expansion during the Last Glacial Maximum (Russell et al., 2014).

millennial-scale variability is only distinctly visible in the Lake Tanganyika record. This suggests a non-linear response of climate variability to global ice sheet evolution in all major centers of deep tropical convection (Russell et al., 2014). The drier LGM conditions in the centers of deep tropical convection have likely led to a reduction in primary productivity and thus a reduction the Dole effect, which contributed to the LGM enrichment in atmospheric $\delta^{18}O$ (Severinghaus et al., 2009).

In terms of biodiversity, the limited savannah expansions we observed during HS probably lasted not long enough to lead to speciation as suggested by the refugia hypothesis (Haffer, 1969). In contrast, it is conceivable that shifts in vegetation cover during HS led to the connection of otherwise separated biomes (Bush, 2017). Phylogenetic and biogeographic studies suggest that the savannah regions to the north and the south of the Amazon basin were repeatedly connected during the Pleistocene (Behling et al., 2009; Da Silva and Bates, 2002; Quijada-Mascareñas et al., 2007). Geographically, the expansion of C4 biomes likely took place in the north-eastern parts of the basin, where a long recognized dry corridor exists under present-day conditions (Behling et al., 2009). We suggest that the opening of migration routes through this dry corridor was influenced by vegetation shifts during HS and was therefore potentially subject to millennial-scale climate variability (Bush, 2017). This may not necessarily have led to a continuous connection, but could have provided stepwise migration routes along savannah patches in the Amazonian interior.

5. Conclusions

Our study shows that the hydrological changes in the lowland Amazon basin are controlled by glacial climate variability. Drying during glacials did, however, not lead to large-scale C4 vegetation expansion. Our study thus supports the hypothesis that Amazonian biodiversity is not a result of forest refugia during glacial droughts, but was rather favored by stable climatic and environmental conditions (Behling et al., 2009; Cheng et al., 2013; Hoorn et al., 2010; Smith et al., 2014). Our finding that the most pronounced C3 to C4 vegetation shifts were associated with HS opens new perspectives in understanding the connection of biomes in the Neotropics.

Concerning the future development of Amazonian vegetation and precipitation, our results suggest that a temperature increase due to current global warming would lead to an overall increased influx of humidity to the Amazon basin and thus to overall potentially larger amounts of precipitation (Gloor et al., 2015). While the Amazon rainforest seems to be stable towards large-scale drying over the lowland basin, meridional displacement of the tropical rain belt led to the most pronounced shifts in vegetation. A northward shift of the tropical rain belt due to more pronounced warming in the northern hemisphere (Friedman et al., 2013) would thus suggest potential savannah expansion in the south of the basin, where, in addition, large-scale deforestation takes place.

Author contributions

SM, CMC and ES conceived the study and led the sampling effort. CH conducted the laboratory work and wrote the manuscript. UM, MP and MS conducted the climate model experiments. All authors contributed to the interpretation of the results.

All data presented in this manuscript is permanently archived on www.pangaea.de.

Acknowledgements

We acknowledge funding through the DFG-Research Center/Cluster of Excellence “The Ocean in the Earth System” at MARUM – Center for Environmental Sciences. CH thanks GLOMAR – Bremen International Graduate School for Marine Sciences for support. CMC acknowledges FAPESP (grant 2012/17517-3), CAPES (grant 564/2015) and CNPq (302607/2016-1) for support. We thank the RV Maria S. Merian cruise MSM20/3 crew for support during sampling, and Ralph Kreutz and Birk Stern for laboratory support. We acknowledge the GeoB Core Repository at MARUM – University of Bremen for supplying the samples used in this study. We thank two anonymous reviewers for their comments and suggestions which greatly improved the manuscript.

Appendix A. Supplementary material

Supplementary material related to this article can be found online at http://dx.doi.org/10.1016/j.epsl.2017.09.013.

References

Absy, M.L., 1991. Mise en évidence de quatre phases d'ouverture de la foret dense dans le sud-est de l'Amazonie au cours des 60 000 dernieres annees. C. R. Acad. Sci. Ser. II 312, 673–678.

Baker, P.A., Fritz, S.C., 2015. Nature and causes of Quaternary climate variation of tropical South America. Quat. Sci. Rev. 124, 31–47.

Behling, H., Bush, M., Hooghiemstra, H., 2009. Biotic development of Quaternary Amazonia: a palynological perspective. In: Amazonia: Landscape and Species Evolution. Wiley–Blackwell Publishing Ltd., pp. 335–345.

Bintanja, R., van de Wal, R.S.W., Oerlemans, J., 2005. Modelled atmospheric temperatures and global sea levels over the past million years. Nature 437, 125–128.

Blaauw, M., Christen, J.A., 2011. Flexible paleoclimate age–depth models using an autoregressive gamma process. Bayesian Anal. 6, 457–474.

Boot, C.S., Ettwein, V.J., Maslin, M.A., Weyhenmeyer, C.E., Pancost, R.D., 2006. A 35,000 year record of terrigenous and marine lipids in Amazon Fan sediments. Org. Geochem. 37, 208–219.

Bouchez, J., Galy, V., Hilton, R.G., Gaillardet, J., Moreira-Turcq, P., Perez, M.A., France-Lanord, C., Maurice, L., 2014. Source, transport and fluxes of Amazon River particulate organic carbon: insights from river sediment depth-profiles. Geochim. Cosmochim. Acta 133, 280–298.

Braconnot, P., Otto-Bliesner, B., Harrison, S., Joussaume, S., Peterchmitt, J.Y., Abe-Ouchi, A., Crucifix, M., Driesschaert, E., Fichefet, T., Hewitt, C.D., Kageyama, M., Kitoh, A., Laîné, A., Loutre, M.F., Marti, O., Merkel, U., Ramstein, G., Valdes, P., Weber, S.L., Yu, Y., Zhao, Y., 2007. Results of PMIP2 coupled simulations of the Mid-Holocene and Last Glacial Maximum – Part 1: experiments and large-scale features. Clim. Past 3, 261–277.

Brienen, R.J.W., Helle, G., Pons, T.L., Guyot, J.L., Gloor, M., 2012. Oxygen isotopes in tree rings are a good proxy for Amazon precipitation and El Nino–Southern Oscillation variability. Proc. Natl. Acad. Sci. USA 109, 16957–16962.

Brienen, R.J.W., Phillips, O.L., Feldpausch, T.R., Gloor, E., Baker, T.R., Lloyd, J., Lopez-Gonzalez, G., Monteagudo-Mendoza, A., Malhi, Y., Lewis, S.L., Vasquez Martinez, R., Alexiades, M., Alvarez Davila, E., Alvarez-Loayza, P., Andrade, A., Aragao, L.E.O.C., Araujo-Murakami, A., Arets, E.J.M.M., Arroyo, L., Aymard, C.G.A., Banki, O.S., Baraloto, C., Barroso, J., Bonal, D., Boot, R.G.A., Camargo, J.L.C., Castilho, C.V., Chama, V., Chao, K.J., Chave, J., Comiskey, J.A., Cornejo Valverde, F., da Costa, L., de Oliveira, E.A., Di Fiore, A., Erwin, T.L., Fauset, S., Forsthofer, M., Galbraith, D.R., Grahame, E.S., Groot, N., Herault, B., Higuchi, N., Honorio Coronado, E.N., Keeling, H., Killeen, T.J., Laurance, W.F., Laurance, S., Licona, J., Magnussen, W.E., Marimon, B.S., Marimon-Junior, B.H., Mendoza, C., Neill, D.A., Nogueira, E.M., Nunez, P., Pallqui Camacho, N.C., Parada, A., Pardo-Molina, G., Peacock, J., Pena-Claros, M., Pickavance, G.C., Pitman, N.C.A., Poorter, L., Prieto, A., Quesada, C.A., Ramirez, F., Ramirez-Angulo, H., Restrepo, Z., Roopsind, A., Rudas, A., Salomao, R.P., Schwarz, M., Silva, N., Silva-Espejo, J.E., Silveira, M., Stropp, J., Talbot, J., ter Steege, H., Teran-Aguilar, J., Terborgh, J., Thomas-Caesar, R., Toledo, M., Torello-Raventos, M., Umetsu, R.K., van der Heijden, G.M.F., van der Hout, P., Guimaraes Vieira, I.C., Vieira, S.A., Vilanova, E., Vos, V.A., Zagt, R.J., 2015. Long-term decline of the Amazon carbon sink. Nature 519, 344–348.

Bush, M.B., 2017. The resilience of Amazonian forests. Nature 541, 167–168.

Carvalho, L.M.V., Jones, C., Liebmann, B., 2004. The South Atlantic convergence zone: intensity, form, persistence, and relationships with intraseasonal to interannual activity and extreme rainfall. J. Climate 17, 88–108.

Castañeda, I.S., Schouten, S., 2011. A review of molecular organic proxies for examining modern and ancient lacustrine environments. Quat. Sci. Rev. 30, 2851–2891.

Chadwick, R., Good, P., Willett, K., 2016. A simple moisture advection model of specific humidity change over land in response to SST warming. J. Climate 29, 7613–7632.

Cheng, H., Sinha, A., Cruz, F.W., Wang, X.F., Edwards, R.L.A., d'Horta, F.M., Ribas, C.C., Vuille, M., Stott, L.D., Auler, A.S., 2013. Climate change patterns in Amazonia and biodiversity. Nat. Commun. 4, 1411.

Colinvaux, P.A., DeOliveira, P.E., Moreno, J.E., Miller, M.C., Bush, M.B., 1996. A long pollen record from lowland Amazonia: forest and cooling in glacial times. Science 274, 85–88.

Colinvaux, P.A., Irion, G., Räsänen, M., Bush, M.B., Nunes De Mello, J.A.S., 2001. A paradigm to be discarded: geological and paleoecological data falsify the HAFFER & PRANCE refuge hypothesis of Amazonian speciation. Amazoniana 16, 609–646.

Collins, W.D., Bitz, C.M., Blackmon, M.L., 2006. The Community Climate System Model version 3 (CCSM3). J. Climate 19, 2122–2143.

Cranwell, P.A., 1981. Diagenesis of free and bound lipids in terrestrial detritus deposited in a lacustrine sediment. Org. Geochem. 3, 79–89.

Damuth, J.E., Flood, R.D., 1983. Morphology, sedimentation processes, and growth pattern of the Amazon Deep-Sea Fan. Geo Mar. Lett. 3, 109–117.

D'Apolito, C., Absy, M.L., Latrubesse, E.M., 2013. The Hill of Six Lakes revisited: new data and re-evaluation of a key Pleistocene Amazon site. Quat. Sci. Rev. 76, 140–155.

Da Silva, J.M.C., Bates, J.M., 2002. Biogeographic patterns and conservation in the South American Cerrado: a tropical Savanna hotspot. Bioscience 52, 225–233.

Deplazes, G., Luckge, A., Peterson, L.C., Timmermann, A., Hamann, Y., Hughen, K.A., Rohl, U., Laj, C., Cane, M.A., Sigman, D.M., Haug, G.H., 2013. Links between tropical rainfall and North Atlantic climate during the last glacial period. Nat. Geosci. 6, 213–217.

Diefendorf, A.F., Mueller, K.E., Wing, S.L., Freeman, K.H., 2010. Global patterns in leaf ^{13}C discrimination and implications for studies of past and future climate. Proc. Natl. Acad. Sci. USA 107, 5738–5743.

Dupont, L.M., Schluetz, F., Ewah, C.T., Jennerjahn, T.C., Paul, A., Behling, H., 2010. Two-step vegetation response to enhanced precipitation in Northeast Brazil during Heinrich event 1. Glob. Change Biol. 16, 1647–1660.

Eglinton, G., Hamilton, R.J., 1967. Leaf epicuticular waxes. Science 156, 1322–1335.

Feakins, S.J., Peters, T., Wu, M.S., Shenkin, A., Salinas, N., Girardin, C.A.J., Bentley, L.P., Blonder, B., Enquist, B.J., Martin, R.E., Asner, G.P., Malhi, Y., 2016. Production of leaf wax n-alkanes across a tropical forest elevation transect. Org. Geochem. 100, 89–100.

Feakins, S.J., Sessions, A.L., 2010. Controls on the D/H ratios of plant leaf waxes in an arid ecosystem. Geochim. Cosmochim. Acta 74, 2128–2141.

Friedman, A.R., Hwang, Y.-T., Chiang, J.C.H., Frierson, D.M.W., 2013. Interhemispheric temperature asymmetry over the twentieth century and in future projections. J. Climate 26, 5419–5433.

Garreaud, R.D., Vuille, M., Compagnucci, R., Marengo, J., 2009. Present-day South American climate. Palaeogeogr. Palaeoclimatol. Palaeoecol. 281, 180–195.

Geyer, W.R., Beardsley, R.C., Lentz, S.J., Candela, J., Limeburner, R., Johns, W.E., Castro, B.M., Soares, I.D., 1996. Physical oceanography of the Amazon shelf. Cont. Shelf Res. 16, 575–616.

Gloor, M., Barichivich, J., Ziv, G., Brienen, R., Schöngart, J., Peylin, P., Ladvocat Cintra, B.B., Feldpausch, T., Phillips, O., Baker, J., 2015. Recent Amazon climate as background for possible ongoing and future changes of Amazon humid forests. Glob. Biogeochem. Cycles 29, 2014GB005080.

Haberle, S.G., Maslin, M.A., 1999. Late Quaternary vegetation and climate change in the Amazon basin based on a 50,000 year pollen record from the Amazon fan, ODP site 932. Quat. Res. 51, 27–38.

Haffer, J., 1969. Speciation in Amazonian forest birds. Science 165, 131–137.

Häggi, C., Sawakuchi, A.O., Chiessi, C.M., Mulitza, S., Mollenhauer, G., Sawakuchi, H.O., Baker, P.A., Zabel, M., Schefuß, E., 2016. Origin, transport and deposition of leaf-wax biomarkers in the Amazon Basin and the adjacent Atlantic. Geochim. Cosmochim. Acta 192, 149–165.

Henry, L.G., McManus, J.F., Curry, W.B., Roberts, N.L., Piotrowski, A.M., Keigwin, L.D., 2016. North Atlantic ocean circulation and abrupt climate change during the last glaciation. Science 353, 470–474. http://dx.doi.org/10.1126/science.aaf5529.

Hessler, I., Dupont, L., Bonnefille, R., Behling, H., Gonzalez, C., Helmens, K.F., Hooghiemstra, H., Lebamba, J., Ledru, M.P., Lezine, A.M., Maley, J., Marret, F., Vincens, A., 2010. Millennialscale changes in vegetation records from tropical Africa and South America during the last glacial. Quat. Sci. Rev. 29, 2882–2899.

Hijmans, R.J., Cameron, S.E., Parra, J.L., Jones, P.G., Jarvis, A., 2005. Very high resolution interpolated climate surfaces for global land areas. Int. J. Climatol. 25, 1965–1978.

Hoorn, C., Wesselingh, F.P., ter Steege, H., Bermudez, M.A., Mora, A., Sevink, J., Sanmartin, I., Sanchez-Meseguer, A., Anderson, C.L., Figueiredo, J.P., Jaramillo, C., Riff, D., Negri, F.R., Hooghiemstra, H., Lundberg, J., Stadler, T., Sarkinen, T., Antonelli, A., 2010. Amazonia through time: Andean uplift, climate change, landscape evolution, and biodiversity. Science 330, 927–931.

Hughen, K.A., Eglinton, T.I., Xu, L., Makou, M., 2004. Abrupt tropical vegetation response to rapid climate changes. Science 304, 1955–1959.

Jaeschke, A., Rühlemann, C., Arz, H., Heil, G., Lohmann, G., 2007. Coupling of millennial-scale changes in sea surface temperature and precipitation off northeastern Brazil with high-latitude climate shifts during the last glacial period. Paleoceanography 22, 2006PA001391.

Kanner, L.C., Burns, S.J., Cheng, H., Edwards, R.L., 2012. High-latitude forcing of the South American summer monsoon during the Last Glacial. Science 335, 570–573.

Latrubesse, E.M., Franzinelli, E., 2005. The late Quaternary evolution of the Negro River, Amazon, Brazil: implications for island and floodplain formation in large anabranching tropical systems. Geomorphology 70, 372–397.

Lee, J.-E., Johnson, K., Fung, I., 2009. Precipitation over South America during the Last Glacial Maximum: an analysis of the "amount effect" with a water isotope-enabled general circulation model. Geophys. Res. Lett. 36.

Lee, S.-Y., Chiang, J.C.H., Chang, P., 2014. Tropical Pacific response to continental ice sheet topography. Clim. Dyn. 44, 2429–2446.

Lippold, J., Luo, Y., Francois, R., Allen, S.E., Gherardi, J., Pichat, S., Hickey, B., Schulz, H., 2012. Strength and geometry of the glacial Atlantic meridional overturning circulation. Nat. Geosci. 5, 813–816.

Loncke, L., Droz, L., Gaullier, V., Basile, C., Patriat, M., Roest, W., 2009. Slope instabilities from echo-character mapping along the French Guiana transform margin and Demerara abyssal plain. Mar. Pet. Geol. 26, 711–723.

Marengo, J.A., Soares, W.R., Saulo, C., Nicolini, M., 2004. Climatology of the low-level jet east of the Andes as derived from the NCEP-NCAR reanalyses: characteristics and temporal variability. J. Climate 17, 2261–2280.

Mayle, F.E., Burbridge, R., Killeen, T.J., 2000. Millennial-scale dynamics of southern Amazonian rain forests. Science 290, 2291–2294.

McManus, J.F., Francois, R., Gherardi, J.M., Keigwin, L.D., Brown-Leger, S., 2004. Collapse and rapid resumption of Atlantic meridional circulation linked to deglacial climate changes. Nature 428, 834–837.

Meade, R.H., Dunne, T., Richey, J.E., De M. Santos, U., Salati, E., 1985. Storage and remobilization of suspended sediment in the lower Amazon River of Brazil. Science 228, 488–490.

Merkel, U., Prange, M., Schulz, M., 2010. ENSO variability and teleconnections during glacial climates. Quat. Sci. Rev. 29, 86–100.

Mosblech, N.A.S., Bush, M.B., Gosling, W.D., Hodell, D., Thomas, L., van Calsteren, P., Correa-Metrio, A., Valencia, B.G., Curtis, J., van Woesik, R., 2012. North Atlantic forcing of Amazonian precipitation during the last ice age. Nat. Geosci. 5, 817–820.

Mulitza, S., Chiessi, C.M., Cruz, A.P.S., Frederichs, T., Gomes, J.G., Gurgel, M.H., Haberkern, J., Huang, E., Jovane, L., Kuhnert, H., Pittauerová, D., Reiners, S.-J., Roud, S.C., Schefuß, E., Schewe, F., Schwenk, T.A., Sicoli Seoane, J.C., Sousa, S.H.M., Wagner, D.J., Wiers, S., 2013. Response of Amazon Sedimentation to Deforestation, Land Use and Climate Variability – Cruise No. MSM20/3 – February 19–March 11, 2012 – Recife (Brazil)–Bridgetown (Barbados). Berichte, Fachbereich Geowissenschaften, Universität Bremen, Bremen, Germany, pp. 1–86.

Olson, D.M., Dinerstein, E., Wikramanayake, E.D., Burgess, N.D., Powell, G.V.N., Underwood, E.C., D'Amico, J.A., Itoua, I., Strand, H.E., Morrison, J.C., Loucks, C.J., Allnutt, T.F., Ricketts, T.H., Kura, Y., Lamoreux, J.F., Wettengel, W.W., Hedao, P.,

Kassem, K.R., 2001. Terrestrial ecoregions of the worlds: a new map of life on Earth. Bioscience 51, 933–938.

Pennington, R.T., Prado, D.E., Pendry, C.A., 2000. Neotropical seasonally dry forests and Quaternary vegetation changes. J. Biogeogr. 27, 261–273.

Ponton, C., West, A.J., Feakins, S.J., Galy, V., 2014. Leaf wax biomarkers in transit record river catchment composition. Geophys. Res. Lett. 41, 6420–6427.

Quijada-Mascareñas, J.A., Ferguson, J.E., Pook, C.E., Salomão, M.D.G., Thorpe, R.S., Wüster, W., 2007. Phylogeographic patterns of trans-Amazonian vicariants and Amazonian biogeography: the Neotropical rattlesnake (Crotalus durissus complex) as an example. J. Biogeogr. 34, 1296–1312.

Reimer, P.J., Bard, E., Bayliss, A., Beck, J.W., Blackwell, P.G., Ramsey, C.B., Buck, C.E., Cheng, H., Edwards, R.L., Friedrich, M., Grootes, P.M., Guilderson, T.P., Haflidason, H., Hajdas, I., Hatte, C., Heaton, T.J., Hoffmann, D.L., Hogg, A.G., Hughen, K.A., Kaiser, K.F., Kromer, B., Manning, S.W., Niu, M., Reimer, R.W., Richards, D.A., Scott, E.M., Southon, J.R., Staff, R.A., Turney, C.S.M., van der Plicht, J., 2013. INTCAL13 and MARINE13 radiocarbon age calibration curves 0–50000 years cal BP. Radiocarbon 55, 1869–1887.

Russell, J.M., Vogel, H., Konecky, B.L., Bijaksana, S., Huang, Y.S., Melles, M., Wattrus, N., Costa, K., King, J.W., 2014. Glacial forcing of central Indonesian hydroclimate since 60,000 y BP. Proc. Natl. Acad. Sci. USA 111, 5100–5105.

Sachse, D., Billault, I., Bowen, G.J., Chikaraishi, Y., Dawson, T.E., Feakins, S.J., Freeman, K.H., Magill, C.R., McInerney, F.A., van der Meer, M.T.J., Polissar, P., Robins, R.J., Sachs, J.P., Schmidt, H.L., Sessions, A.L., White, J.W.C., West, J.B., Kahmen, A., 2012. Molecular paleohydrology: interpreting the hydrogen-isotopic composition of lipid biomarkers from photosynthesizing organisms. Annu. Rev. Earth Planet. Sci. 40, 221–249.

Sbrocco, E.J., Barber, P.H., 2013. MARSPEC: ocean climate layers for marine spatial ecology. Ecology 94, 979.

Schefuß, E., Schouten, S., Schneider, R.R., 2005. Climatic controls on central African hydrology during the past 20,000 yr. Nature 437, 1003–1006.

Severinghaus, J.P., Beaudette, R., Headly, M.A., Taylor, K., Brook, E.J., 2009. Oxygen-18 of O-2 records the impact of abrupt climate change on the terrestrial biosphere. Science 324, 1431–1434.

Smith, B.T., McCormack, J.E., Cuervo, A.M., Hickerson, M.J., Aleixo, A., Cadena, C.D., Perez-Eman, J., Burney, C.W., Xie, X., Harvey, M.G., Faircloth, B.C., Glenn, T.C., Derryberry, E.P., Prejean, J., Fields, S., Brumfield, R.T., 2014. The drivers of tropical speciation. Nature 515, 406–409.

Tierney, J.E., deMenocal, P.B., 2013. Abrupt shifts in Horn of Africa hydroclimate since the last glacial maximum. Science 342, 843–846.

Tierney, J.E., Russell, J.M., Huang, Y., Sinninghe Damsté, J.S., Hopmans, E.C., Cohen, A.S., 2008. Northern hemisphere controls on tropical Southeast African climate during the past 60,000 years. Science 322, 252–255.

van der Hammen, T., Duivenvoorden, J.F., Lips, J.M., Urrego, L.E., Espejo, N., 1992. Late Quaternary of the middle Caquetá River area (Colombian Amazonia). J. Quat. Sci. 7, 45–55.

van der Merwe, N.J., Medina, E., 1991. The canopy effect, carbon isotope ratios and foodwebs in Amazonia. J. Archaeol. Sci. 18, 249–259.

Vecchi, G.A., Soden, B.J., 2007. Global warming and the weakening of the tropical circulation. J. Climate 20, 4316–4340.

Vizy, E.K., Cook, K.H., 2007. Relationship between Amazon and high Andes rainfall. J. Geophys. Res. 112, D07107.

Vuille, M., Bradley, R.S., Werner, M., Healy, R., Keimig, F., 2003. Modeling δ18O in precipitation over the tropical Americas: 1. Interannual variability and climatic controls. J. Geophys. Res., Atmos. 108, 4174.

Wang, X., Edwards, R.L., Auler, A.S., Cheng, H., Kong, X., Wang, Y., Cruz, F.W., Dorale, J.A., Chiang, H.-W., 2017. Hydroclimate changes across the Amazon lowlands over the past 45,000 years. Nature 541, 204–207.

Werth, D., Avissar, R., 2002. The local and global effects of Amazon deforestation. J. Geophys. Res., Atmos. 107, 8087.

Yeager, S.G., Shields, C.A., Large, W.G., Hack, J.J., 2006. The low-resolution CCSM3. J. Climate 19, 2545–2566.

Zhang, Y.C., Chiessi, C.M., Mulitza, S., Zabel, M., Trindade, R.I.F., Hollanda, M., Dantas, E.L., Govin, A., Tiedemann, R., Wefer, G., 2015. Origin of increased terrigenous supply to the NE South American continental margin during Heinrich Stadial 1 and the Younger Dryas. Earth Planet. Sci. Lett. 432, 493–500.